Asymmetric Phase Effects and Mantle Convection Patterns

Mian Liu

Recent high-pressure experiments and thermodynamic calculations have shown that the Clapeyron slope of the spinel-perovskite phase transition at a depth of 660 kilometers in the Earth's mantle changes from negative to positive at temperatures above 1700° to 2000°C. In numerical experiments that account for this phase behavior, cold downwelling flows were impeded at the phase boundary, but hot plumes ascended to the upper mantle with ease. The resultant mantle convection was partially layered and strongly time-dependent. Mantle layering was weaker when the mantle was hotter and when the Rayleigh number was larger.

Whether convection in the Earth's mantle occurs in a single layer (*1*) or in two layers separated at the seismic discontinuity at 660-km depth (*2*) is uncertain. This seismic discontinuity corresponds to the solid-state mineral transition between spinel and perovskite structures (*3*). At temperatures below 2000°C, this phase boundary has a negative Clapeyron slope ($dP/dT < 0$, where P is pressure and T is temperature), and the density jump across the phase boundary is nearly 10% (*4*). Such a phase boundary tends to inhibit mantle convection because of the lateral density contrast induced by the distortion of the phase boundary in the hot upwelling and cold downwelling mantle flows (Fig. 1) (*5*).

Most models are based on the assumption of a constant negative Clapeyron slope for this phase boundary in the entire pressure-temperature domain (*6*). Recent studies (*7–9*) of mineral phase relations in the upper mantle, however, suggest that the Clapeyron slope of the spinel-perovskite phase boundary changes to positive at temperatures above 1700° to 2000°C (Fig. 2). Most of the results are for the $(Mg,Fe)_2SiO_4$ phases, because olivine is probably the dominant mineral in the upper mantle (*10*). Kato and Kumazawa (8) have shown that, for a lherzolitic mantle, which is likely more representative of the real mantle composition, the sign change of the Clapeyron slope occurs at ~1700°C (Fig. 2). The fact that the Clapeyron slope changes from negative to positive in the normal temperature range of the mantle at 660-km depth (Fig. 2) suggests that hot upwelling mantle plumes, which may have a core temperature 300°C higher than the ambient mantle (*11*), may cross the spinel-perovskite phase boundary where the Clapeyron slope is positive (Fig. 2) and thus encounter no phase-related resistance (see Fig. 1). Cold subducting slabs, on the other hand, will meet the phase boundary characterized by a negative Clapeyron slope and thus be impeded.

I investigated the temperature-dependent asymmetric phase effects on mantle convection in a two-dimensional finite difference model with the extended Boussinesq approximation (*12, 13*). In this approximation, the density of the mantle is assumed to be constant except for thermally induced variations in ascending and descending mantle flows and density contrast associated with the displacement of phase boundaries. The approximation also accounts for the effects of adiabatic cooling and viscous dissipation. This formula allows for complicated phase boundaries that are difficult to model in anelastic compressible models (*14*). The nondimensional momentum equation is given by

$$\nabla^4\psi = Ra\,\frac{\partial T}{\partial x} - f(T,P)\cdot Rb\,\frac{\partial T}{\partial x} \qquad (1)$$

where ψ is the stream function and x is the spatial variable in the horizontal direction. The parameter Ra ($\alpha g\rho_0\Delta T d^3/\kappa\eta$) is the background thermal Rayleigh number, essentially the ratio of thermal buoyancy force to viscous resistance. The parameter Rb ($\Delta\rho g d^3/\kappa\eta$) is the local phase Rayleigh number associated with phase transitions. The function $f(T,P)$ describes the distribution of the local buoyancy forces resulting from lateral density variations associated with distortion of the phase boundary (Fig. 1). These local buoyancy forces may be approximated by a sheet of anomalous mass at the phase boundary. The thickness of the anomalous mass sheet is given by the product of the Clapeyron slope and the lateral temperature contrast (see Fig. 1). The distortion of the spinel-perovskite phase boundary in the Earth's mantle is less than 60 km (*15*), which is more than one order of magnitude smaller than the characteristic length scale of the convection model. Thus, the details of the phase boundary distortion may be neglected as a first approximation. I assume the distortion of the phase boundary to be 60 km in the core of upwelling and downwelling flows.

The equation of energy conservation in the extended Boussinesq approximation takes the form

$$\frac{\partial T}{\partial t} = \frac{1}{\overline{C}_p(T,z)}\left[\nabla^2 T + wD_0\alpha(T+T_0) + R + \frac{D_0}{Ra}\tau_{ij}\frac{\partial u_i}{\partial x_j}\right] - \mathbf{u}\cdot\nabla T - \sum_{i=1}^{k} w\,\frac{\overline{\Delta H_i f_i}}{\delta z} \qquad (2)$$

where $\overline{C}_p$ is the effective specific heat scaled by its surface value, w is the vertical velocity, $\mathbf{u}$ is the velocity vector, τ_{ij} is the

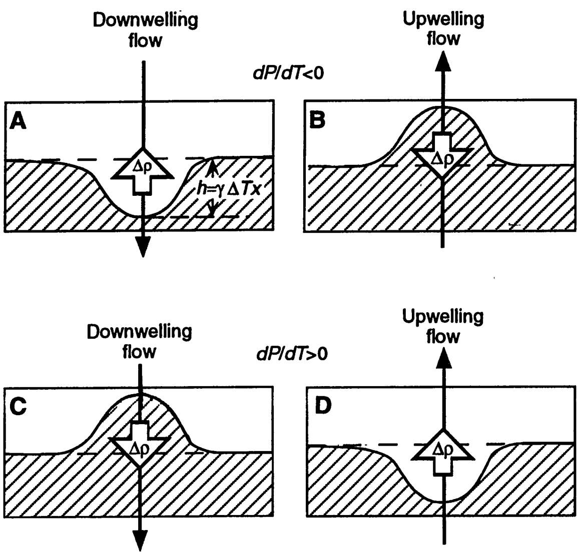

Fig. 1. Schematic illustration of local buoyancy forces (shown by the empty arrows marked with a $\Delta\rho$) induced by displacement of the phase boundary. Solid arrows show the direction of mantle flows. The hatched area is the denser phase. When the Clapeyron slope is negative ($dP/dT < 0$), the phase boundary is displaced (**A**) downward (to higher pressure) in the cold downwelling flow and (**B**) upward in the hot upwelling flow (to lower pressure), causing a lateral density contrast. The local buoyancy forces thus induced tend to inhibit mantle circulation, as indicated by their opposite direction to that of the mantle flows. The amount of phase boundary distortion (h) is given by the product of the Clapeyron slope (γ) and the lateral temperature contrast (ΔTx). On the other hand, mantle flows are facilitated at the phase boundary when the Clapeyron slope is positive (**C** and **D**).

Department of Geological Sciences, University of Missouri, Columbia, MO 65211, USA.

deviatoric stress, D_0 is the dissipation number based on surface values (16), δ_z is a characteristic thickness of the phase boundary, T_0 is the nondimensional surface temperature, R is the internal heating parameter for a bottom-heated configuration (17), and $\overline{\Delta H_t}$ is the nondimensionalized latent heat associated with phase transitions (13, 18). The latent heat is calculated for a Clapeyron slope of −4 MPa/K, an upper limit of experimental results (19).

The governing equations were integrated over time with the finite difference method (13, 20). The boundary conditions were fixed temperatures at the top and the bottom (Table 1). Periodic boundary conditions were used along the vertical edges. The thickness of the model convection layer was taken to be 1500 km for a better spatial resolution. Most numerical experiments were conducted with a 100 by 100 grid. For a two-dimensional box with an aspect ratio of one (vertical) to three (horizontal), the spatial resolution is 15 km vertically and 45 km horizontally. Final results were verified with a finer, 150 by 150 grid.

Numerical experiments were conducted systematically to investigate the asymmetric phase effects on mantle convection patterns, which are illustrated by the comparison of two cases in Fig. 3. In case 1, I assumed a simple spinel-perovskite phase boundary with a constant negative Clapeyron slope, whereas in case 2 the Clapeyron slope changes from negative to zero at temperatures above 1800°C, or 0.6 of the dimensionless temperature (Fig. 3). Both cases started with an upwelling and a downwelling flow approaching the phase boundary at 660 km. As the mantle flows reached the phase boundary (t_1 in Fig. 3), both ascending and descending flows were impeded in case 1, whereas in case 2 the core of the hot upwelling flow was able to cross the phase boundary. The result in case 2 occurred because at temperatures above 1800°C, the Clapeyron slope was zero, and thus the flow did not encounter phase-related resistance. After one to two overturns (t_2 in Fig. 3), a clear mantle layering developed in case 1. On the other hand, convection in case 2 was more complicated: While some hot upwelling flows crossed the phase boundary with ease, others were inhibited because cold downwelling material accumulated above the phase boundary. The convection regime was partially layered and strongly time-dependent. The cold upper mantle material that accumulated above the phase boundary periodically flushed into the lower mantle when sufficient negative buoyancy force accumulated. Hot upwelling flows, on the other hand, often broke through the phase boundary to form discrete diapirs. After four to five overturns (t_3 in Fig. 3), a relatively strong mantle layering developed in case 1, whereas in case 2 the convection patterns were characterized by strong dynamic instabilities at the phase boundary and relatively weak mantle layering (mainly resistance to the downwelling cold flows). Despite simplifications involved in the model, these results indicate that the pattern of mantle convection is sensitive to the asymmetric phase effects.

Temperature-dependent asymmetric phase effects may have played a significant role in the evolution of mantle convection over the Earth's cooling history. Mantle dynamics in the Archean, 4.5 to 2.5 billion years ago, are not well understood, but it is likely that the Rayleigh number was greater in the past. Two sets of numerical experiments, cases 3 and 4, illustrate the phase effects at a larger Rayleigh number (Fig. 3). Case 3 is the same as case 1, except the Rayleigh number is now five times as large (5×10^6). It is clear from comparison of case 3 and case 1 that layering in the mantle is stronger at a larger Rayleigh number. Similar results were observed in earlier studies (12, 13, 18), which have led some authors to suggest that the Archean mantle was strongly layered (18).

Such conclusions, however, may not be valid if the temperature-dependent asymmetric phase effects are included. Case 4 (Fig. 3) is similar to case 2 but with a Rayleigh number five times larger ($Ra = 5 \times 10^6$). The temperature at which the Clapeyron slope of the spinel-perovskite phase boundary changes from negative to zero is lowered by 200°C in case 4 (to 1600°C) to simulate the asymmetric phase effects in the Archean mantle, which was probably a few hundred degrees hotter than that at present. A weak layering was shown at the beginning of the numerical experiments as cold downwelling flows were impeded at the phase boundary, whereas hot upwelling plumes crossed the phase boundary with little resistance (t_1 in Fig. 3). The flow quickly evolved into strongly time-dependent and complicated patterns (t_2 in Fig. 3). After four to five overturns (t_3 in Fig. 3), little layering was left.

The Archean mantle was also characterized by relatively high rates of internal

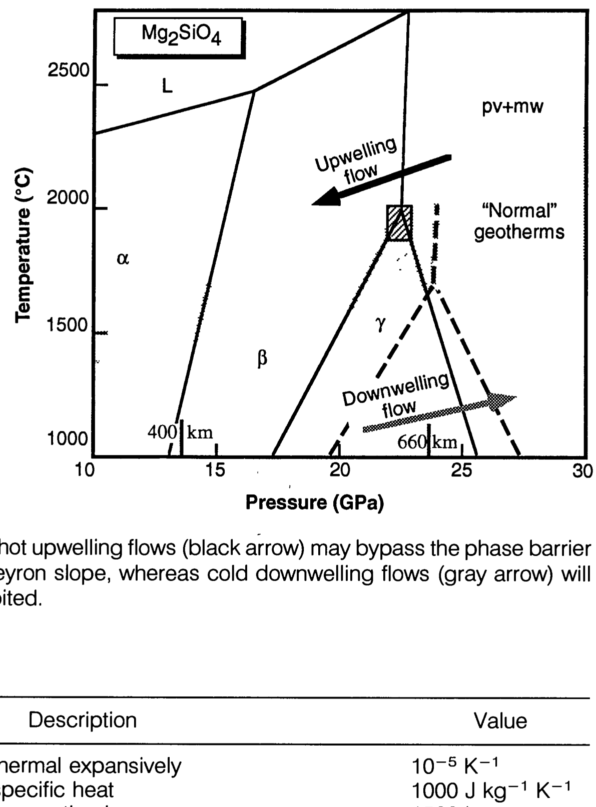

Fig. 2. Phase relations of Mg_2SiO_4 phases in the upper mantle. Phases are olivine (α), β-phase spinel (β), spinel (γ), perovskite (pv), magnesiowüstite (mw), and liquid (L). Phase boundaries are based mainly on (9). Note that the negative Clapeyron slope of the spinel-perovskite phase boundary changes to slightly positive at the triple point around 2000°C. The shaded square indicates the temperature range of the triple point from (7, 8). The triple point lies in a considerably lower temperature (1700°C) in a lherzolitic mantle composition, as indicated by the phase boundaries in dashed lines (8). Note that the change of the Clapeyron slope occurs in the normal temperature range of the mantle [from (4)]. Thus, hot upwelling flows (black arrow) may bypass the phase barrier characterized by the negative Clapeyron slope, whereas cold downwelling flows (gray arrow) will meet the phase barrier and be inhibited.

Table 1. Model parameters.

Parameter	Description	Value
α	Background thermal expansively	10^{-5} K^{-1}
C_p	Background specific heat	1000 J kg^{-1} K^{-1}
d	Depth of the convection layer	1500 km
ΔT	Temperature drop across the layer	2500°C
T_0	Temperature at the top of the layer	500°C
D_0	Dissipation number	0.3
ρ_0	Background mantle density	3500 kg m^{-3}
$\Delta\rho$	Density change across the phase boundary	350 kg m^{-3}
g	Gravitational acceleration	10 m s^{-2}
δz	Dimensionless thickness of phase boundary	0.01 (15 km)
t	Time nondimensionalized by thermal diffusion across the convection layer	0.001 (71.4 million years ago)

heating by radioactive decay. The numerical results indicated that the effect of internal heating was similar to that of increased Rayleigh number: With internal heating, mantle layering became stronger when a simple phase boundary was assumed but weaker when the asymmetric phase effects were included. The use of a positive Clapeyron slope at high temperature also predicted a weaker mantle layering.

Although the two-dimensional model used in this work is adequate to capture the basic physics of asymmetric phase effects, convection in the Earth's mantle is clearly three-dimensional (*21*). Because hot upwelling mantle plumes are mainly caused by basal heating and the total mass of inferred mantle plumes is much smaller than that of subducting slabs, only a small fraction of the slabs need to be returned to the lower mantle to keep the mass balance. In addition, the ascension of plumes to the upper mantle may not force overturns of the mantle as strong as those shown in Fig. 3. Different chemical composition (*22*) or viscosity (*23*) of the upper and lower mantle may also cause layered convection.

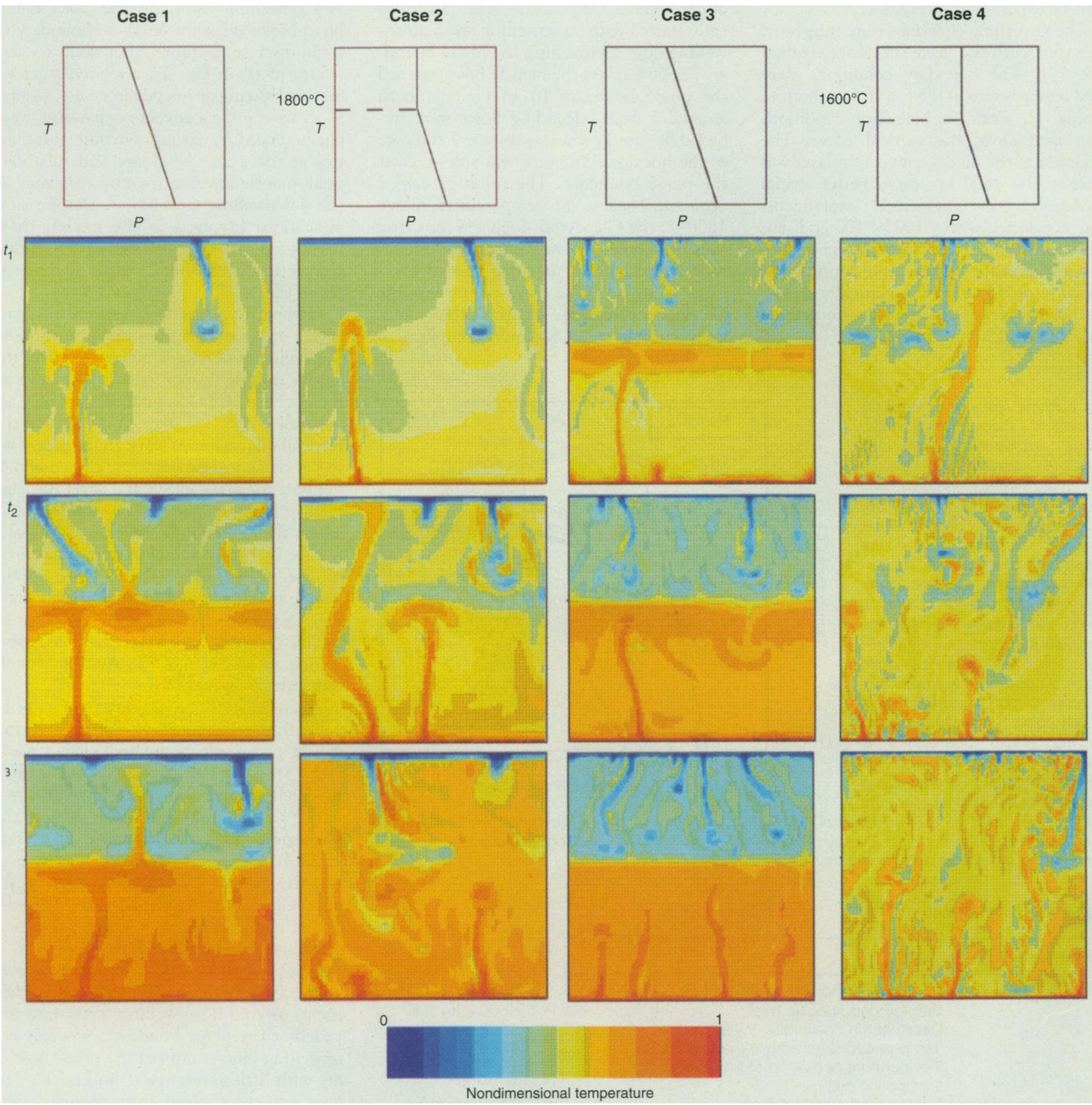

Fig. 3. Numerically simulated evolution of the thermal field in the mantle. The top panels show schematically the spinel-perovskite phase boundary used in each case (tick marks indicate a depth of 660 km). The color images of each column are sequential snapshots of the thermal field. The aspect ratio is 3 (horizontal) to 1 (vertical). The Rayleigh numbers are 1×10^6 for cases 1 and 2 and 5×10^6 for cases 3 and 4. For cases 1 and 2, the nondimensional time t_1 (2.5×10^{-4}) is at the beginning of the experiment, t_2 (1.5×10^{-3}) is after one to two overturns, and t_3 (4×10^{-3}) is after four to five overturns. For cases 3 and 4, t_1 (2×10^{-4}) is after one to two overturns, t_2 (4×10^{-4}) is after two to three overturns, and t_3 (8×10^{-4}) is after four to five overturns.

REFERENCES AND NOTES

1. G. F. Davies, *J. Geophys. Res.* **89**, 6017 (1984); K. C. Creager and T. H. Jordan, *ibid.* **91**, 3573 (1986); J. Phipps Morgan and P. M. Shearer, *Nature* **365**, 506 (1993).
2. D. P. McKenzie, J. M. Roberts, N. O. Weiss, *J. Fluid Mech.* **62**, 465 (1974); F. M. Richter and D. P. McKenzie, *J. Geophys.* **44**, 441 (1978).
3. C. R. Bina, *Rev. Geophys.* (suppl.) **29** (1991).
4. D. L. Anderson, *J. Geophys. Res.* **92**, 13968 (1987).
5. Other phase effects include latent heat that is either absorbed (endothermic) or released (exothermic) during phase transitions. The effects of latent heat are generally in the sense opposite to that of the local body forces associated with the distortion of phase boundaries [G. Schubert, D. A. Yuen, D. L. Turcotte, *Geophys. J. R. Astron. Soc.* **42**, 705 (1975)]. However, the dynamic effects of latent heat and other phase effects are usually much smaller than the buoyancy force induced by phase-boundary distortion (*12*).
6. Although multiple phase boundaries were considered in (*13*) and some follow-up studies [(*18*); S. Honda, D. A. Yuen, S. Balachandar, D. Reuteler, *Science* **259**, 1308 (1993)], a number of errors in the implementation of phase effects, including the limiting of the phase-related body forces to the phase boundary, prevented significant asymmetric phase effects from being seen.
7. R. Bohler and A. Chopelas, *Geophys. Res. Lett.* **18**, 1147 (1991).
8. T. Kato and M. Kumazawa, in *Dynamic Processes of Material Transformation in the Earth's Interior*, M. Marumo, Ed. (Terra, Tokyo, 1990), pp. 277–208.
9. Y. Fei, S. K. Saxena, A. Navrotsky, *J. Geophys. Res.* **95**, 6915 (1990).
10. A. E. Ringwood, in *The Earth, Its Origin, Structure and Evolution*, M. W. McElhinny, Ed. (Academic Press, New York, 1979), pp. 1–58.
11. M. Liu and C. G. Chase, *J. Geophys. Res.* **94**, 5571 (1989); M. McNutt, *Geophys. Monogr. Am. Geophys. Union* **43**, 1 (1987).
12. U. R. Christensen and D. A. Yuen, *J. Geophys. Res.* **90**, 10291 (1985).
13. M. Liu, D. A. Yuen, W. Zhao, S. Honda, *Science* **252**, 1836 (1991).
14. P. Machetel and P. Weber, *Nature* **350**, 55 (1991); L. P. Solheim and W. R. Peltier, *Can. J. Earth Sci.* **30**, 881 (1993).
15. C. W. Wicks Jr. and M. A. Richards, *Science* **261**, 1424 (1993).
16. G. T. Jarvis and D. P. McKenzie, *J. Fluid Mech.* **96**, 515 (1980).
17. S. A. Weinstein, P. L. Olson, D. A. Yuen, *Geophys. Astrophys. Fluid Dyn.* **47**, 157 (1989).
18. W. L. Zhao, D. A. Yuen, S. Honda, *Phys. Earth Planet. Inter.* **72**, 185 (1992).
19. E. Ito and E. Takahashi, *J. Geophys. Res.* **94**, 10637 (1989).
20. S. Honda and D. A. Yuen, *Earth Planet. Sci. Lett.* **96**, 349 (1990).
21. P. J. Tackley, D. J. Stevenson, G. A. Glatzmaier, G. Schubert, *Nature* **361**, 699 (1993).
22. D. L. Anderson and J. Bass, *ibid.* **320**, 321 (1986); R. Jeanloz and E. Knittle, *Philos. Trans. R. Soc. London Ser. A* **328**, 417 (1989).
23. B. H. Hager and M. A. Richards, *Philos. Trans. R. Soc. London Ser. A* **328**, 309 (1989).

24. Supported by the Research Board of the University of Missouri. I thank C. Chase, J. Engeln, and P. Nabelek for reading an early version of the manuscript.

8 February 1994; accepted 10 May 1994

African *Homo erectus*: Old Radiometric Ages and Young Oldowan Assemblages in the Middle Awash Valley, Ethiopia

J. D. Clark,* J. de Heinzelin, K. D. Schick, W. K. Hart, T. D. White, G. WoldeGabriel, R. C. Walter, G. Suwa, B. Asfaw, E. Vrba, Y. H.-Selassie

Fossils and artifacts recovered from the middle Awash Valley of Ethiopia's Afar depression sample the Middle Pleistocene transition from *Homo erectus* to *Homo sapiens*. Ar/Ar ages, biostratigraphy, and tephrachronology from this area indicate that the Pleistocene Bodo hominid cranium and newer specimens are approximately 0.6 million years old. Only Oldowan chopper and flake assemblages are present in the lower stratigraphic units, but Acheulean bifacial artifacts are consistently prevalent and widespread in directly overlying deposits. This technological transition is related to a shift in sedimentary regime, supporting the hypothesis that Middle Pleistocene Oldowan assemblages represent a behavioral facies of the Acheulean industrial complex.

A *Homo* cranium was found at Bodo, Middle Awash Valley, in Ethiopia's Afar in 1976 (*1*). An age of ~350,000 years for this fossil and stratigraphically associated Acheulean artifacts has been widely assumed based on their morphologies (*2*), but in the absence of radiometric dating. A second hominid's parietal was found in 1981 (BOD-VP-1/1) (*3, 4*) and a distal humerus fragment was recovered in 1990 (BOD-VP-1/2). These specimens straddle the traditional morphological interface between *Homo erectus* and *Homo sapiens*—a transition whose age is poorly defined. The Bodo cranium exhibits cut marks indicating defleshing (*5*). This specimen is usually referred to as "archaic" *Homo sapiens*, as have other inadequately dated specimens from Europe (Arago, Petralona) and Asia (Yunxian).

We recently recovered additional Middle Pleistocene vertebrate fossils at Bodo. In this report, we establish chronostratigraphic control for deposits at Bodo and elucidate the relations between Oldowan and Acheulean assemblages widely distributed in this area. We do not follow a previous stratigraphic framework formulated for the Middle Awash (*6, 7*) because of the difficulty in correlating sedimentary units across a broad region marked by considerable faulting and lacking precise chronometric control. Our fieldwork concentrated on Middle Pleistocene archaeological and paleontological occurrences extending across the modern Bodo, Dawaitoli, and Hargufia catchments (Fig. 1). These are incorporated in fluvial sediments derived from wadis or seasonal rivers on the eastern side of the basin and a major river along the basin axis. These Middle Pleistocene deposits are in fault contact with a sequence of Lower Pleistocene and Pliocene deposits to the east. The Middle Pleistocene deposits are succeeded by a formation exposed as a fault block to the west that bears typical Middle Stone Age artifacts provisionally attributed to the Late Pleistocene.

Most of the in situ Middle Pleistocene deposits in the Bodo-Hargufia area are in a sedimentary unit now informally designated "u" (Fig. 1). This ~35-m-thick package comprises four cyclical sedimentary units and is divided into subunits u1 to u4 (u4 is typically truncated by later erosion). Each subunit consists of gravel sand to clay silt with calcic soils and concretions at the top. Sand and silt of u1 and u2 are indicative of deposition in a stabilized alluvial plain. Those of u3 and u4 reflect increasingly shifting silty overbank and sandy channel deposits. A normal fault (fault 6) to the west separates u1 to u4 from a 15- to 20-m-thick sequence of deposits that appears to represent the continuation of unit u. We informally designate the latter beds as unit u-t. These beds contain abundant Middle Pleistocene vertebrate fossils including the three fossil hominids from the upper Bodo sand unit (UBSU) (*1*). They

J. D. Clark, T. D. White, Y. H.-Selassie, Laboratory for Human Evolutionary Studies, Department of Anthropology, University of California, Berkeley, CA 94720, USA.
J. de Heinzelin, Institut Royal des Sciences Naturelles de Belgique, 1040 Brussels, Belgium.
K. D. Schick, Department of Anthropology, Indiana University, Bloomington, IN 47405, USA.
W. K. Hart, Department of Geology, Miami University, Oxford, OH 45056, USA.
G. WoldeGabriel, EES-1/D462, Los Alamos National Laboratory, Los Alamos, NM 87545, USA.
R. C. Walter, Geochronology Center, Institute of Human Origins, Berkeley, CA 94709, USA.
G. Suwa, Department of Anthropology, University of Tokyo, 113 Tokyo, Japan.
B. Asfaw, Post Office Box 5717, Addis Ababa, Ethiopia.
E. Vrba, Department of Geology and Geophysics, Yale University, New Haven, CT 06511, USA.

*To whom correspondence should be addressed.